Real-time and Multichannel Measurement of Contractility of hiPSC-Derived 3D Skeletal Muscle using Fiber Optics-Based Sensing

Alessandro Iuliano, Matthias Haalstra, Ramkumar Raghuraman, Kevin Bielawski, Anjali P. Bholasing, Erik van der Wal, Jessica C. de Greef, and W. W. M. Pim Pijnappel*

As the field of cardiac and skeletal muscle tissue engineering expands, so does the need for accurate and reliable systems to generate in vitro 3D tissues and analyze their functional properties. In this study, the Cuore is introduced, a system that integrates sensors based on optical fibers and uses the principle of light interferometry to detect the contraction of 3D Tissue Engineered Skeletal Muscles (3D-TESMs). The technology employed in the Cuore allows for reproducible and multichannel force measurements down to a nano-Newtons resolution while maintaining sterility and permitting continuous non-invasive recording within and outside standard tissue culture incubators. Thanks to the integrated electrodes for electrical pulse stimulation (EPS), 3D-TESMs generated from three independent hiPSC-derived myogenic progenitors (MPs) lines are stimulated and the contractility is recorded over the course of a week. Through the modulation of different EPS parameters, the optimal combination to induce the 3D-TESMs in producing fully fused tetani without causing damage is determined. Furthermore, 3D-TESMs from different lines exhibit characteristic signatures of spontaneous contractility and response to caffeine, verapamil, and the β-agonist clenbuterol. The ease of use, high sensitivity, and the integrated electrodes and sensors make the Cuore an ideal technology to investigate the biology of contractile tissues and their response to drugs.

1. Introduction

Tissue-engineered 3D constructs of skeletal and cardiac muscle are rapidly becoming standard in vitro models used by researchers alongside traditional 2D cultures and animal models.[1] The popularity of these model systems is explained by the considerable advantages that they carry over the standard cell culture ones, from the improved quality, differentiation potential, and survival to the ability to perform functional studies otherwise impossible in 2D.[1] Specifically, measurement of contractility, either spontaneously occurring or induced by Electrical Pulse Stimulation EPS, is a key feature in studying cardiac and skeletal muscle biology and disease. To this end, numerous recent publications represent the efforts of researchers to optimize platforms for skeletal and cardiac muscle-on-chip. These devices often employ flexible pillars or cantilevers as tendon-like anchor points for the attachment of the contractile tissues.[2–5] The flexible anchors allow the tissue to freely contract and provide the tension required for their proper alignment and differentiation. We recently published an easy method based on 3D printing to fabricate a great number of PDMS chips featuring flexible pillars,[6] which we used to generate 3D Tissue Engineered Skeletal Muscles (3D-TESMs). We subsequently used the platform to explore the contractile properties of 3D-TESMs generated using myogenic progenitors (MPs) derived from human induced pluripotent stem cells (hiPSCs).[7–9] Although they offer numerous benefits over

A. Iuliano, A. P. Bholasing, W. W. M. P. Pijnappel
Department of Clinical Genetics
Erasmus MC University Medical Center
3015 GE Rotterdam, Netherlands
E-mail: w.pijnappel@erasmusmc.nl

A. Iuliano, A. P. Bholasing, W. W. M. P. Pijnappel
Department of Pediatrics
Erasmus MC University Medical Center
3015 GE Rotterdam, Netherlands

A. Iuliano, A. P. Bholasing, W. W. M. P. Pijnappel
Center for Lysosomal and Metabolic Diseases
Erasmus MC University Medical Center
3015 GE Rotterdam, Netherlands

M. Haalstra, R. Raghuraman, K. Bielawski
Optics11 Life
Amsterdam 1101 BM, Netherlands

E. van der Wal, J. C. de Greef
Department of Human Genetics
Leiden University Medical Center
Leiden 2333 ZA, Netherlands

the approaches that use force transducers,[10–14] such as non-destructive and repetitive measurements, these systems usually lack power regarding the throughput and sensitivity of the force measurement component. They often rely on video imaging approaches to record the pillar displacement,[2–5] which requires video-analysis tools to extract meaningful information. This can be a cumbersome process that most importantly lacks accuracy and the possibility to scale up the data acquisition and elaboration. Furthermore, using force transducers or video imaging requires the user to perform the stimulations and measurements outside of the incubator, which results in an end-point analysis and induces cellular stress caused by temperature change, thus affecting real-time measurements of the response to treatments. Here, we present the Cuore: a cantilever-based system compatible with 24 well plates that use integrated optical sensing and EPS for continuous stimulation and real-time recording of contractile activity of engineered tissues. The technology uses light interferometry[15,16] and optical fibers for unprecedented sensitivity, being capable of measuring contractions with a nano Newton resolution.[15] In addition, because of the multiplexing nature of optical fibers, it allows the simultaneous multichannel recording of four tissues at a time. With the Cuore, we performed continuous force measurements of 3D-TESMs generated using three independent MPs lines. Thanks to the closed-lid format and the integrated electrodes and sensors, force measurements could be performed inside a standard incubator, thus maintaining the tissues in a physiological environment. We detected specific time- and line-dependent patterns of contractility, either spontaneous or EPS-induced. We acutely or chronically administered drugs such as caffeine, verapamil, and clenbuterol to modulate the force production of the 3D-TESMs, observing short- and longer-term changes in the curve traces of twitch and tetanic contractions. The technology here presented allows the production and analysis of advanced in vitro systems to model biology, disease, and drug response of contractile tissues.

2. Results

2.1. Measuring Contraction Using Optical-Fibers Technology

The functional unit of the Cuore is the Tissue Sensing Unit (TSU, **Figure 1**A), which is designed to fit inside a well of a 24-well plate and is based on the principle of cantilevers/pillars tendon-like attachment points.[2,17] Two flat, stainless-steel cantilevers of different thicknesses with a rectangular cross-section end with semi-cylindrical tips that provide a larger surface area for an efficient attachment of 3D-TESMs. The other elements of the TSU include the 3D-TESMs generation chamber and the optical fiber sensor (Figure 1A). The PDMS chamber facilitates the formation of spindle-shaped 3D-TESMs (Figure 1B, Figure S1A, Supporting Information). When an electrical field is applied to a 3D-TESM, a concentric contraction is allowed thanks to the flexibility of the thin cantilever, while the thicker one provides an unmovable anchor point (Figure 1B). The optical fiber sensor permits the tracking of the cantilever displacement induced by the tissue contraction (Figure 1C). The positioning of the tip, facing the portion of the cantilever that undergoes the least deflection, provides a strategic advantage: it allows for efficient detection of movement

even in cases where the end of the cantilever is subjected to vibrations caused by the environment. After the signal is produced and sensed, it is transmitted to the integration hardware that filters the signal to be subsequently analyzed (Figure 1D, Materials and Methods).

2.2. The Cuore Smartlid: An Ultra-Sensitive and Multi-Channel System

One of the advantages of optical fiber technology is multi-channeling: a light source can split and propagate its signal through multiple reflective paths, represented by the fiber optics in the Cuore sensing component (Figure S1, Supporting Information). The Cuore was therefore equipped to measure the multiple signals coming from a 24-well plate. (**Figure 2**A, Figure S2A,B, Supporting Information). In accordance with this principle, the system was designed to be a fully integrated culture device that includes, next to the sensing component, an electrode board for stimulation of 3D-TESMs and a closing see-through lid to provide an enclosed and sterile environment that can be fully operated both inside and outside the incubator (Figure 2A). After the formation of the tissues, the 24-well plate equipped with the PDMS chambers can be removed to allow the insertion of the electrode board (Figure 2B, Figure S2B, Supporting Information).

Parameters such as peak force, time-to-peak force, and relaxation time can be extrapolated from the real-time recordings (Figure 2C). Because of the continuous nature of light, optical fiber sensors can record a continuous signal at elevated scanning frequencies,[15,16] reaching thousands of inputs per second (Figure 2C,D). The remarkable sensitivity allows for a nano-Newton resolution, which is able to distinguish even particularly small contraction patterns caused by spontaneous isometric twitches (Figure 2D).

2.3. Generation of hiPSC-derived 3D-TESMs from Three Independent Lines

To assess the functioning of the Cuore we made use of three independent hiPSC lines derived from healthy individuals, which underwent myogenic differentiation according to an optimization of our previously published protocol.[8,18,9] The resulting MPs were used to generate 3D-TESMs (**Figure 3**A) which showed the presence of long, multinucleated, and striated myotubes upon induction of fusion (Figure 3B, Figure S3A, Supporting Information). The immunostaining for the sarcomeric protein titin highlights intrinsic morphologic differences among the three lines, with line 1 displaying the highest myogenic potential as exemplified by the presence of thicker and more densely packed myotubes at D14 post-fusion (Figure 3C). To assess the functional capabilities of the 3D-TESMs, we proceeded to measure contractile force every other day, starting from D7 post-differentiation, induced upon Electrical Pulse Stimulation (EPS), until D14 (see Figure 3A for outline).

**ADVANCED
SCIENCE NEWS**

www.advancedsciencenews.com

**ADVANCED
MATERIALS
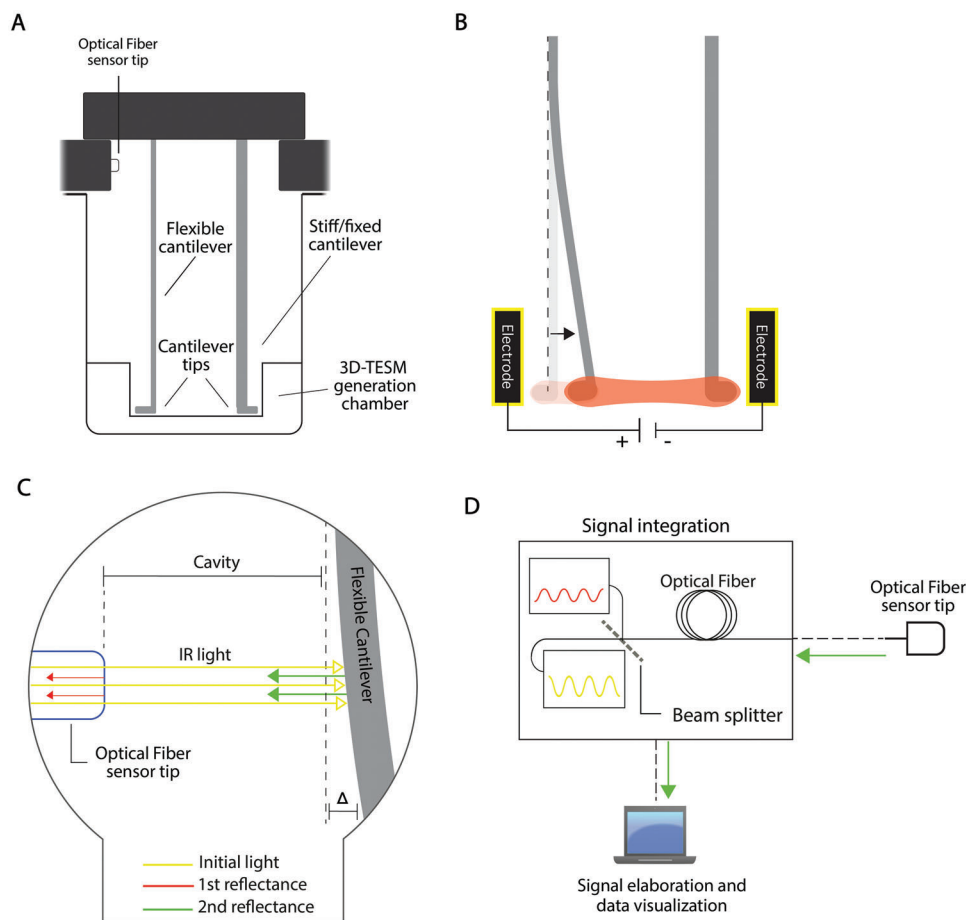TECHNOLOGIES**

www.advmattechnol.de

Figure 1. Optical fibers-based technology to measure contractility of engineered skeletal muscle tissues. A) Scheme of a Tissue Sensing Unit (TSU): a functional basic unit for allowing the generation of 3D-TESMs and measurement of contractility. One unmovable, thicker cantilever and a thinner, flexible cantilever serve as tendon-like attachment points for contractile tissues. B) Scheme of Electrical Pulse Stimulation (EPS)-induced contraction of a 3D-TESM. C,D) Schematic representation of the general principle of light-based sensing employed in the system: infra-red light coming from the fiber optics is reflected on the moving cantilever and sensed back, the signal is then integrated in the hardware, filtered and elaborated using computer software to produce real-time data.

2.4. Characterization of 3D-TESM Contractile Properties Upon Electrical Stimulation

First, we evaluated the contractile properties of the 3D-TESMs using the integrated electrical stimulation and sensing capabilities of the Cuore. Thanks to the real-time high sensitivity of the system, it was possible to track even the most subtle changes in contractility (**Figure 4**). Furthermore, because of its incubator-friendly format, it was possible to assess the tissue's behavior without any possible stresses coming from moving the 3D-TESMs to non-physiological environments. We decided to find the optimal combination of electrical parameters to be used for EPS, by assessing ramps of increasing voltages, pulse amplitudes, and frequencies, with the goal to obtain a full and sustained tetanic contraction. We initially tested a combination of 2 V, 2 ms pulse duration, and a ramp of 20 Hz to 75 Hz on line 1, which proved to be visibly inadequate to produce a fused tetanus (Figure S3B, Supporting Information). We then proceeded to increase the pulse duration to 5 ms, while maintaining the same voltage. This resulted in a slightly higher force at lower frequen-

cies while maintaining the proportional increase with higher frequencies to a maximum of 75 Hz (Figure 4A). By extending the pulse duration even more to 10 ms we saw a considerable increase in absolute force, with virtually non-existent differences among the different frequencies, suggesting that we may have reached a plateau state for the amplitude parameter (Figure 4B). Consequentially, and since the shape of the contraction curve was still considered not ideal, we continued by increasing the voltage to 3.5 V. This produced the most visible change in both force output and shape of the curve, with the clear induction of fused tetanus (Figure 4C). Here, the different frequencies produced still a similar force output, with 50 Hz surprisingly yielding the highest absolute force. We eventually proceeded to increase the voltage to up to 5 V, resulting in almost a doubled force and the emergence of a distinct pattern among the different frequencies (Figure 4D). Remarkably, the 50 Hz stimulus proved again to be the strongest, surpassing 75 Hz, which was assessed at the level of 30 Hz, but higher than 20 Hz. Finally, the last step to evaluate the suitability of the combination of parameters we found was to determine if 3D-TESMs could tolerate such contractions for a
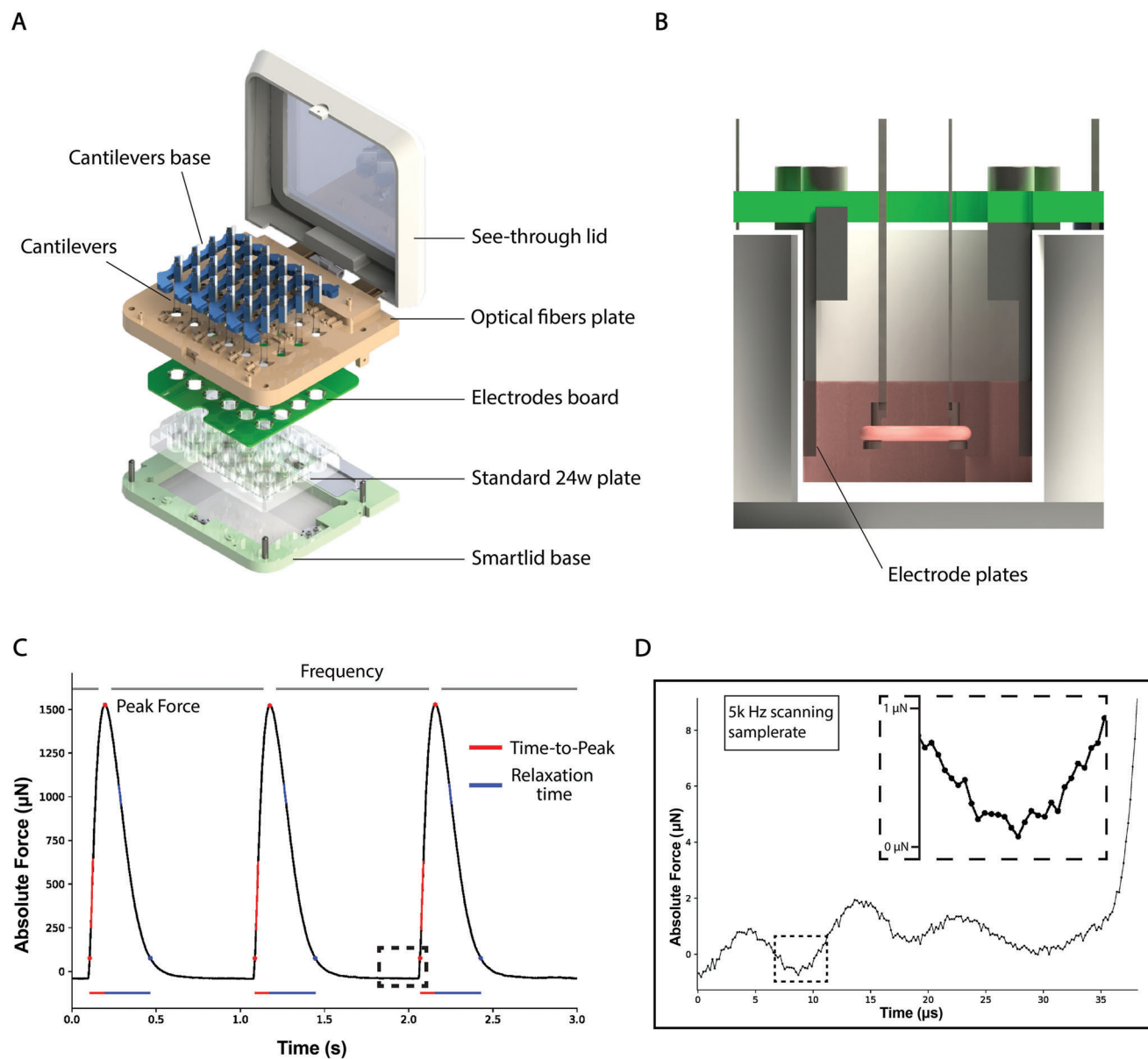
Figure 2. The Cuore: a multi-channel integrated system with high sensitivity. A) Exploded view rendering of the Cuore Smartlid. The system is designed to be compatible with a 24 well plate, integrates a board with 24 couples of carbon electrodes, and a see-through lid that encloses the device. B) Rendering of one TSU with a 3D-TESM, the two carbon electrodes are positioned parallel to the main longitudinal axis of the tissue. C) Representative visualization of three contraction curves with 1 Hz frequency. From each curve, it is possible to extrapolate several parameters such as peak force, time-to-peak force, and relaxation time. D) Dashed lines insert from (C), zoomed-in: the high sensitivity of the sensors allows to record thousands of points per second, making it possible to detect even small, isometric-like twitches.

prolonged period of time without suffering excessive fatigue. We therefore induced a train of 5 V, 10 ms, and 50 Hz tetanic contractions for 30 min with 20 s intervals (Figure 4E). 3D-TESMs showed a slight, progressive decrease in force, which settled at an average of $\approx$ 90% of initial force after 30 min (Figure 4F, Figure S3E, Supporting Information). We confirmed these results by performing the same characterization on the additional lines (Figure S3C–E, Supporting Information), which showed a comparable effect in both force outputs and contraction curve morphologies. We, therefore, concluded that 5 V amplitude and

10 ms pulse duration with a 50 Hz excitation frequency were the ideal EPS parameters needed to evoke a complete but not excessive excitation-contraction coupling response in 3D-TESMs. To have further proof of the accuracy of the technology, we compared the contraction signal recorded with the Cuore with a measurement of Ca^{2+} flux evoked by EPS and recorded with live fluorescence imaging. After incubating the 3D-TESMs with the labeled calcium indicator Fluo-4, we induced trains of tetanic contractions and performed live imaging while at the same time recording the contraction with the Cuore (Figure 4G,H). The curve
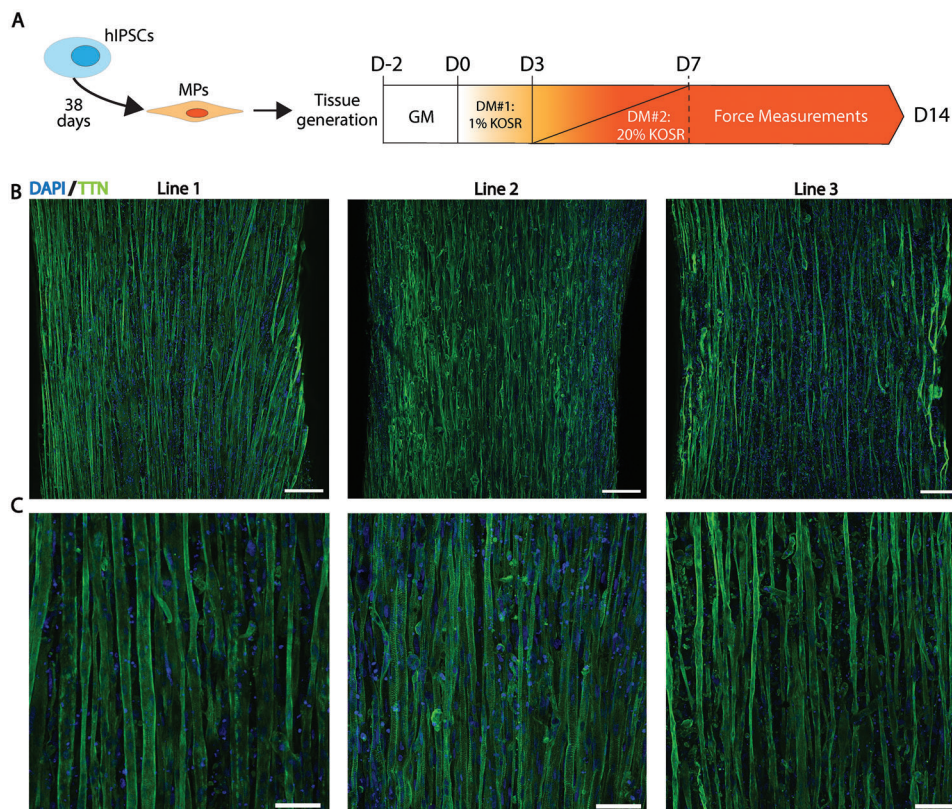
Figure 3. Generation of 3D-TESMs from three different hiPSC-derived lines. A) Schematic timeline for the generation of 3D-TESMs. Human iPSCs underwent a transgene-free, small molecules-based myogenic differentiation protocol to generate myogenic progenitors (MPs). MPs were used to produce engineered tissues using a fibrin/Matrigel hydrogel. Tissues were let differentiate and were cultivated for 14 days, during which the contractile force was measured every other day. B) Immunostaining for the sarcomeric protein titin (green) and DAPI (blue) of the three independent MPs lines used in the study. Scale bars 200 μm. C) Higher magnification of (B), where the morphology and striation of the myotubes are appreciable. Scale bars 50 μm.

obtained with the Cuore closely matched the Ca^{2+} one (Figure 4G). A difference in the relaxation portion of the curve was visible, which highlights the peculiarity of the different physiological dynamics: complete calcium re-uptake from the cytosol to the sarcoplasmic reticulum (SR) has a slower dynamic compared to the sarcomeric relaxation. Therefore, the tissue (and the cantilever to which is anchored) returns to the resting-state length before the Ca^{2+} signal returns back to the baseline, pre-EPS levels.

2.5. 3D-TESMs From Different Lines Show Distinct Contraction Dynamics Over Time

After unraveling the optimal EPS protocol, we then used it to measure twitch and tetanic contraction force for the three lines studied, starting from D7 post-differentiation and over the course of a week (**Figure 5**A,B). Quantification of twitch force revealed similarities but also distinct behaviors among the three lines (Figure 5A). They differed not only in the maximal force reached but also in the time frame needed to reach it. Lines 1 and 2 followed a parabolic-like trend over the course of the recorded period, while line 3 followed a more sinusoidal-like trend. All three lines started with comparable force levels at D7 which progres-

sively increased, with line 1 becoming significantly stronger than the other two already at D9 and reaching its maximum strength at D11, in a similar way to line 2. Line 3 instead reached its maximal twitch force at D13. All lines decreased their twitch force from their maximal output, although settling at D14 to a value higher than the original force at D7. Similar trends were produced also for their tetanic contraction force (Figure 5B). Line 1 reached its peak at D11 and progressively decreased its strength until D14, following a parabolic trend. Line 2 reached its peak tetanic force between D11 and D13 and settled for a slightly lower level at D14. Line 3 linearly increased its force until D13, remaining stable until D14 and ending stronger than the other two lines. When measuring time-to-peak twitch force, however, lines 2 and 3 followed an almost identical trend in terms of values and courses, while line 1′s trend significantly differed from the other two lines and resembled that of its contraction force (Figure 5C).

2.6. Asynchronous Contractility is a Line- and Time-Dependent Feature of 3D-TESMs

By applying the same EPS parameters (10 ms, 5 V pulses) to produce trains of 1 Hz twitch contractions lasting 30 seconds or more, we observed a recurring behavior displayed by the
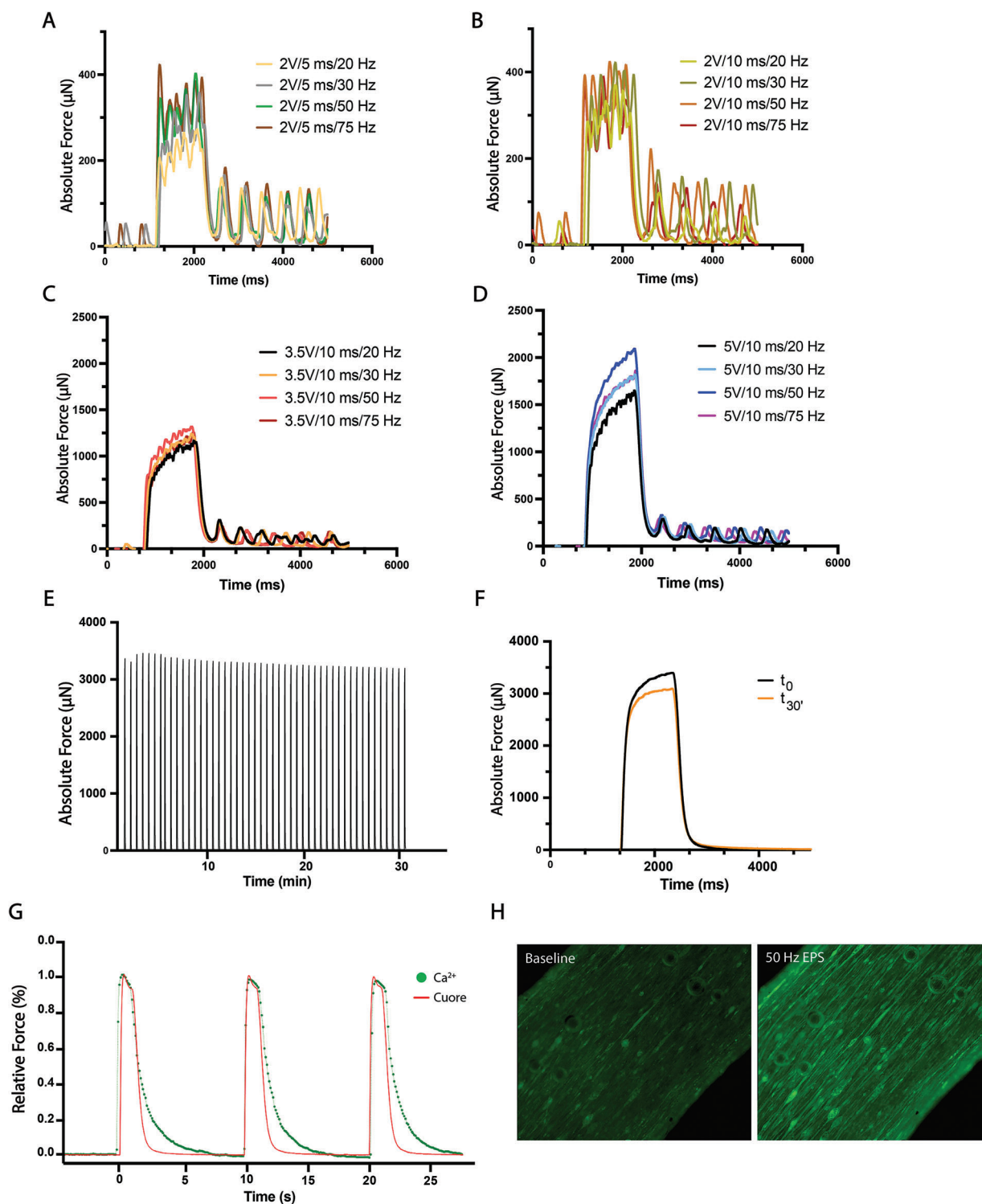
Figure 4. Characterization of 3D-TESMs contractile properties upon Electrical Pulse Stimulation. A-D) Representative contraction curves from line 1, obtained with different combinations of EPS parameters at D7 post-differentiation. A) 2 V, 5 ms pulse duration, and 20 Hz to 75 Hz frequencies ramp produce unfused tetani with increasing absolute force, followed by a sequence of weaker spontaneous twitches. B) 2 V, 10 ms EPS induces slightly stronger contractions, with no clear difference among different frequencies. C) Increasing the voltage to 3.5 V induces fused tetani and triplicates the peak force. D) A further increase to 5 V produces even stronger tetani, with 50 Hz causing the strongest contraction. E) A 30 min train of tetanic contractions induced with 5 V, 10 ms pulses, 50 Hz EPS. F) Overlay of the first tetanus (t_0, in black) and the last tetanus ($t_{30'}$, in orange): a small reduction in force output is observed. G) Overlay of a curve of tetanic contractions recorded with the Cuore (in red), with a curve generated by quantifying the fluorescence signal of Ca^{2+} flux (green dots). H) Frame shots of different time points during live imaging of fluorescence Ca^{2+} flux: baseline fluorescence on the left and on the right a signal recorded during a 50 Hz EPS.
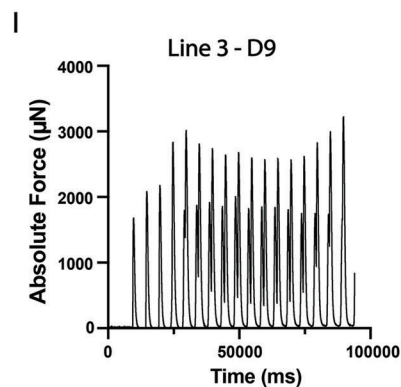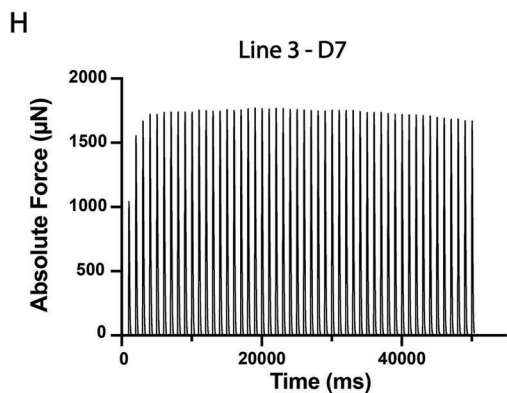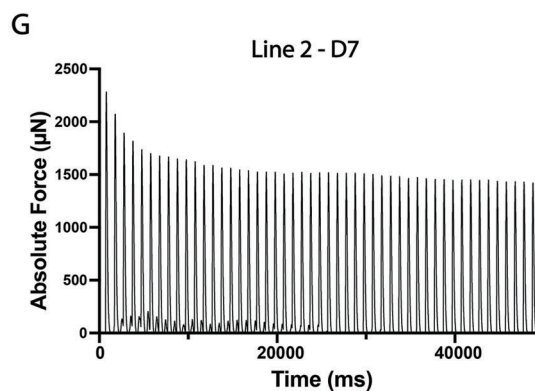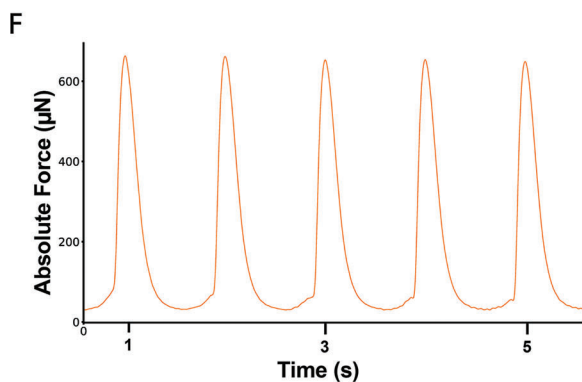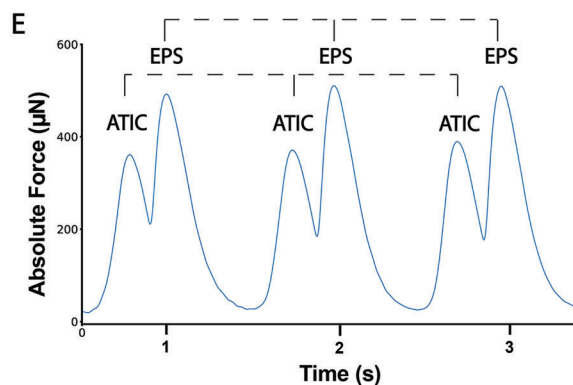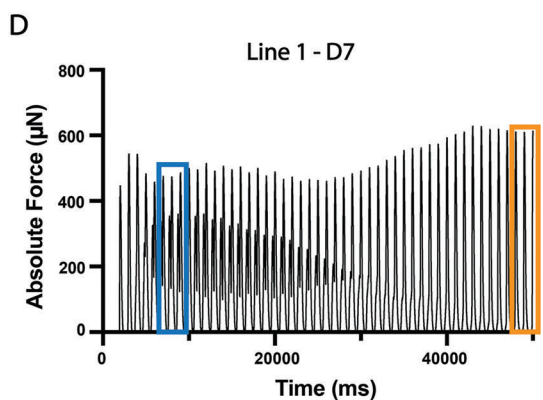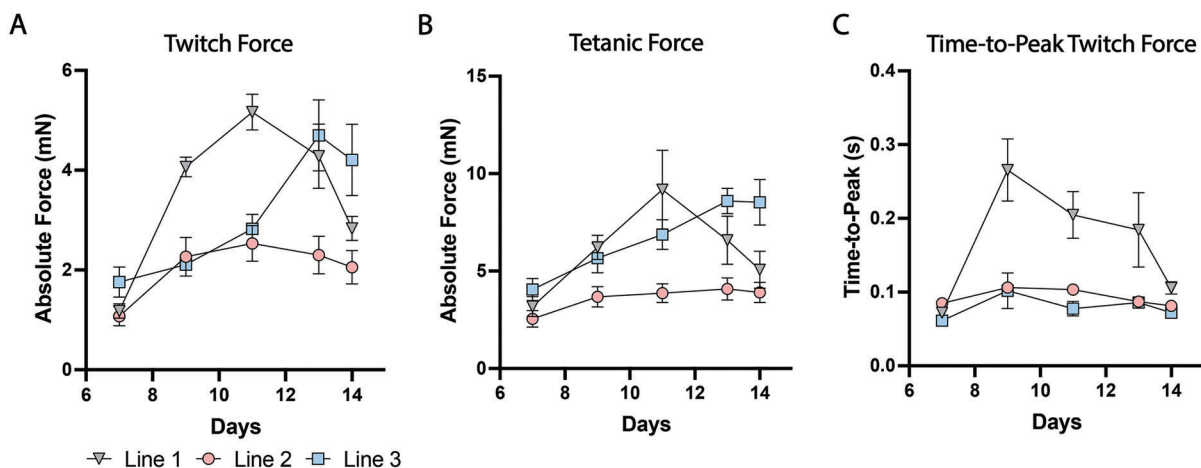
3D-TESMs: the transient appearance of asynchronous contractions (Figure 5D). We identified what we called Asynchronous Twitch-Induced Contractions (ATICs), as additional and spontaneous twitch-like contractions appearing usually after a few EPS-induced twitches and disappearing after 30–40 seconds (Figure 5D). ATICs appear as twitches with variable peak force but at generally lower forces than the EPS-induced ones, they follow a 1 Hz frequency among each other but are close to the EPS-induced twitch to the point of being almost fused with them (Figure 5E). Interestingly, in line 1, once the ATICs disappeared, the EPS-induced contractions increased their peak force (Figure 5F). However, this phenomenon was not necessarily emerging at the same time points for the three lines. Line 1 showed the presence of ATICs initially at D7, as well as line 2 (Figure 5G). Line 3 showed no sign of ATICs at D7 (Figure 5H), but instead manifested them for the first time at D9 (Figure 5I). In the same way as line 1, also for line 3, it seems that the disappearance of ATICs coincided with a subsequent increase in force of the EPS-induced twitches. ATICs continued to be recorded for multiple days, and on the last day of recording (D14) were still exhibited by lines 1 and 3, but not by line 2 (Figure S4E–G, Supporting Information).

2.7. The Cuore Allows for Real-Time Tracking of Drug Effects

We then wanted to test if the real-time sensing of contraction could offer advantages also for drug testing. We decided to use drugs whose acute effects on force production could be potentially assessed in a short time frame. Caffeine[19–27,9] and verapamil[28,29,9] have opposite effects on calcium dynamics in muscle fibers. Caffeine is an agonist of the ryanodine receptor (RyR) on the SR, inducing a greater calcium flux towards the cytosol and therefore ultimately promoting higher contraction forces. Verapamil instead has antagonist effects on the dihydropyridine receptor (DHPR), a voltage-gated calcium channel on the sarcolemma of the muscle fiber. At micromolar concentrations, verapamil can reduce the response of DHPR to voltage-dependent membrane depolarization, which in turn reduces the calcium flux from the SR. We previously showed that caffeine and verapamil can significantly increase and decrease, respectively, the contractile force of 3D-TESMs.[9] However, we were not able to track the temporal changes in force production because of the nature of the video imaging technique employed. Here we show that 100 µM caffeine induces a progressive increase in absolute twitch force from 3D-TESMs of line 1, reaching a plateau state between 25 and 30 min after administration (**Figure 6**A,B). A subsequent increase of caffeine to 1 mM induced a further progressive increase in force, lasting up to 10 min, to eventually settle at another plateau (Figure 6A). A sequential administration of 1 µM verapamil induced an initial decrease in force, counteracting the effect of caffeine, that endured stably for ≈20 min (Figure 6A,B). Once the concentration of verapamil was increased to 10 µM, a steep and linear decrease in force was observed, which resulted in a 50% loss of twitch strength within 15 min of recording (Figure 6A,C).

2.8. 3D-TESMs From Different Lines Show Variable Acute Responses to Caffeine And Clenbuterol

When we tested the effects of drugs on the 3D-TESMs generated from all three lines used in this study at D14 post-differentiation, we observed interesting line-dependent effects. After administration of 100 µM caffeine, line 1 followed a similar behavior as shown D7 (**Figure 7**A,D) with a ≈20% force increase, line 2 showed a remarkable 3-fold force increase compared to baseline (Figure 7B, D), and line 3 a ≈40% force increase (Figure 7C, D). Interestingly, 3D-TESMs generated from line 2 had generally the lowest peak force during the whole week of recording (Figure 5A,B), but showed the highest increase and the highest absolute twitch force upon caffeine stimulation. Clenbuterol is a long-acting b2-adrenergic agonist used in the past as a bronchodilator to treat asthma and is currently approved only as a veterinary drug in many countries,[30] but it has also been classified as an anabolic doping agent.[31,32] However, its use remains controversial as its effects as a performance-enhancing drug have never been fully confirmed. Moreover, known long-term side effects include muscle weakness and weight loss.[33–41] Nevertheless, given its b2-adrenergic agonist properties to rapidly modulate the calcium fluxes in the cell[35,38,39] we decided to test it on the 3D-TESMs from the three different lines. We measured the change in maximal tetanic force after acute administration of 50 µM clenbuterol at D7. The drug induced a dramatic drop in absolute force down to 30% of the initial force for Line 1 (Figure 7E) and even to 20% for line 2 (Figure 7F) 10 min after administration. Line 3 instead saw a reduction in maximal tetanic force of only 25% (Figure 7G). Interestingly, all lines showed a complete recovery in force production after washout, with line 3 displaying even a significant increase of up to 160% of its initial force (Figure 7E-G). The acute effect of clenbuterol on tetanic contractions is visible not only on force output but also on the shape of the tetanus curve itself. Previous studies showed how acute administration of clenbuterol on excised rat muscles induced changes in calcium fluxes that resulted in abnormal tetanic calcium traces.[35] Here, a similar phenomenon could be

---

Figure 5. Peak force, time-to-peak force, and asynchronous contractions are line- and time-dependent features of 3D-TESMs. A, B) Absolute twitch and tetanic force (mN) produced by the three lines of MPs-derived 3D-TESMs from D7 to D14 post-differentiation. The three lines show a clear time-dependent variation in maximal force production, with peaks reached at different time points for the three lines. $n = 8$. C) Quantification of time-to-peak twitch force (ms) for the three lines: while lines 2 and 3 have a similar trend, line 1 behaves differently. $n = 8$. (* = line 1 versus lines 2–3, $p < 0.05$; # = line 2 versus line 3, $p < 0.05$). D) Representative force curves showing detection of asynchronous patterns of contractility upon trains of 1 Hz EPS in line 1 at D7 post-differentiation. E) Zoom-in from the blue insert in (D): EPS-induced contractions are preceded by weaker Asynchronous Twitch-Induced Contractions (ATICs) at the same frequency, forming spontaneous "double peaks". F) Zoom-in from the orange insert in (D): Once the spontaneous peaks disappear, the EPS-evoked peak force increases. G) Representative contraction curves from line 2, which displays similar behavior to line 1, although with lower force ATICS and without a force increase after their disappearance. H) Representative contraction curves from line 3: The asynchronous pattern is not detected at D7. I) The asynchronous pattern is detected at D9 and similarly to line 1, at the disappearance of the ATICS, the EPS-induced force increases.
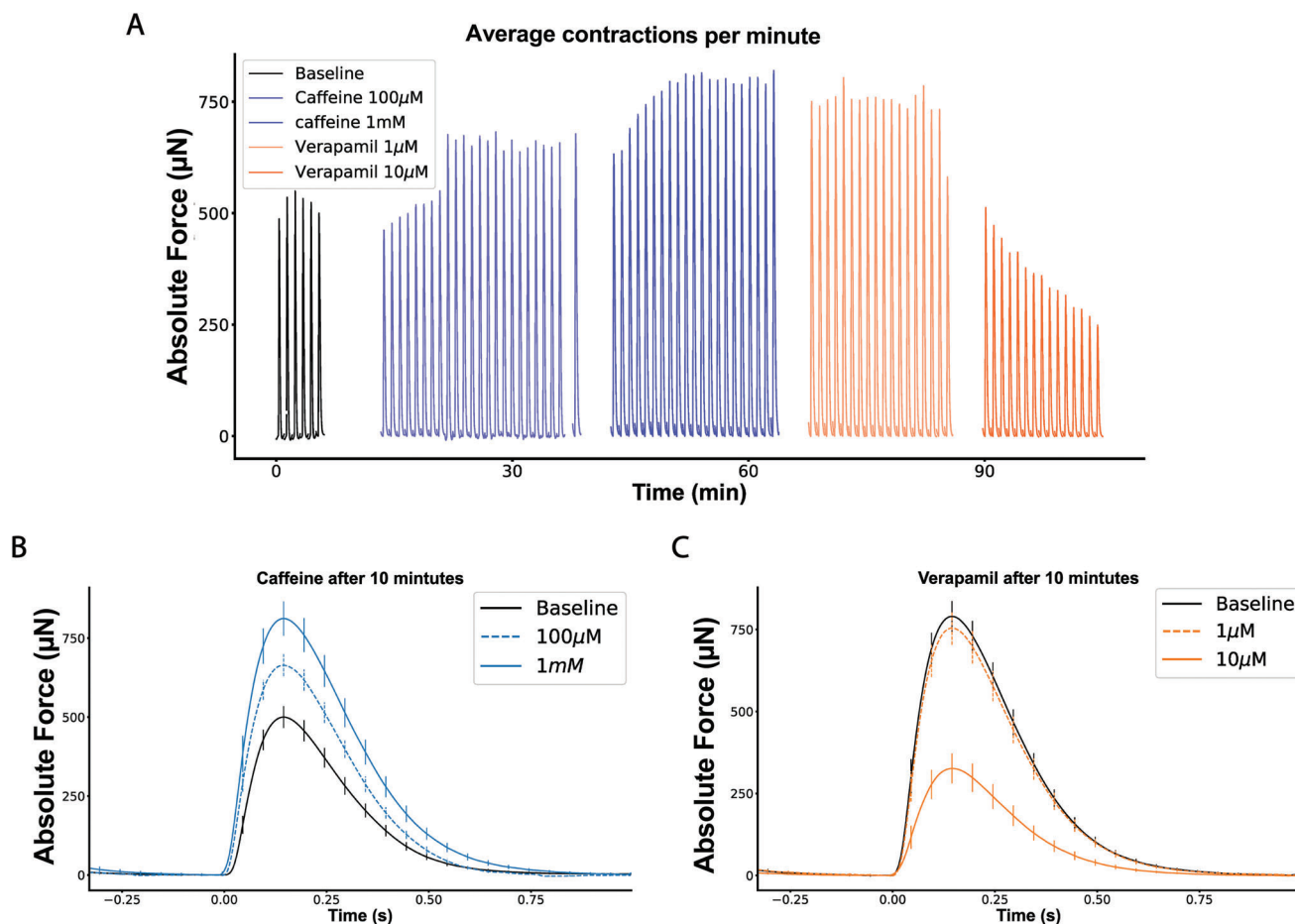

Figure 6. Time- and dose-dependent effects of drugs are tracked in real-time using the Cuore. A) Twitch contraction curves from line 1 tracked for 1 h upon sequential administration of different concentrations of caffeine (purple-blue traces) and verapamil (orange-red) at D7 post-differentiation. The progressive increase in force from baseline after administration of 100 µM and 1 mM caffeine is stopped by the administration of 1 µM verapamil and counter-effected by 10 µM. Gaps between different groups of curves are due to the time required for the administration of the drug (B, C) Overlaps of single twitch curves for baseline/caffeine and baseline/verapamil.

observed in the contraction curves thanks to the high sensitivity of the Cuore system (Figure 7H-J). The tetanus curve resulting after clenbuterol treatment showed a peculiar "sagging" shape:[35] EPS-induced tetani immediately reached their peak, followed by a progressive decay until complete relaxation. After washout the shape of the curve appeared to be back to pre-treatment state, indicating that the effect on the tetanus curve shape is dependent on clenbuterol and that the acute effect is reversible when applied transiently.

2.9. Chronic Treatment with Clenbuterol Induces Distinct Patterns of Force Reduction in 3D-TESMs From Different Lines

After assessing the acute effects of clenbuterol, we tested the impact of reiterated administrations of the drug on 3D-TESMs from the three lines over the course of a week. The contractile force was measured every other day, starting from D7 post-differentiation, immediately before medium exchange containing 10 µM clenbuterol. We observed a different effect of chronic

clenbuterol treatment on the three MPs lines (**Figure 8**). Line 1 showed an initial sharp decline in force measured at the first time point, D9, both in twitch (Figure 8A) and tetanus (Figure 8D). After this time point the force progressively increased back to a level either slightly higher than D7 for twitch or slightly lower for tetanus. Line 2 instead saw a continuous decrease in both twitch (Figure 8B) and tetanic force (Figure 8E) until D11-12, before seeing a slight increase from D13. Line 3 showed again a different trend over time, with twitch force not showing any visible decline before D11, after which it started to linearly and sharply decline to pre-treatment levels (Figure 8C). Tetanic force instead followed a trend initially similar to what was shown by line 1, with a decline at D9, followed by a minimal recovery and a further decline (Figure 8F). The effect of chronic clenbuterol treatment can also be observed when analyzing the tetani curves (Figure 8G-I), where their shapes directly correlate with the amount of force produced. Line 1, which showed the best force recovery over time, also showed a gradual re-shaping of the tetanus curve from the sagged one of D9 to a state more similar to pre-treatment (Figure 8G). Line 2 and 3 instead maintained their sagged curve
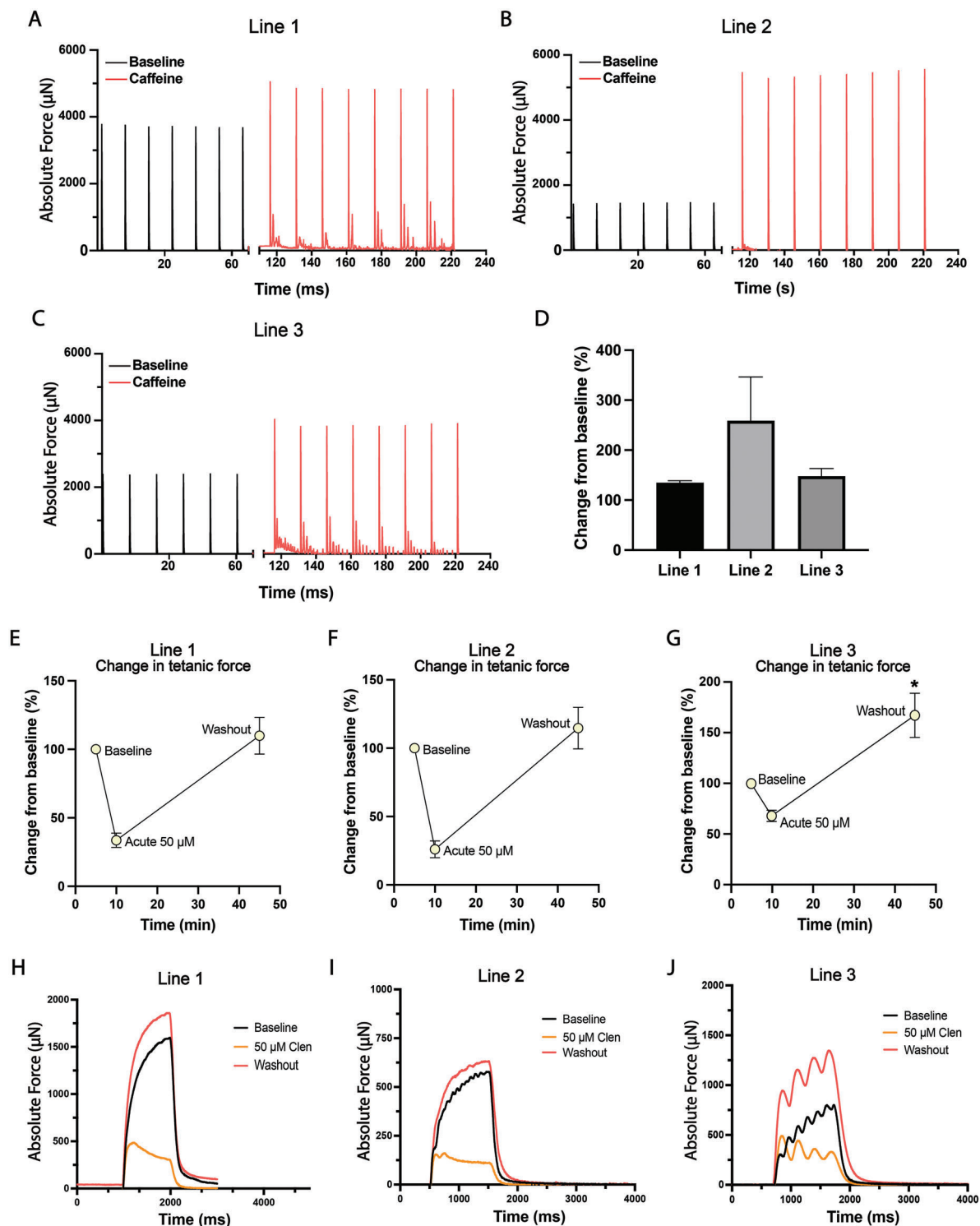
ADVANCED
SCIENCE NEWS

www.advancedsciencenews.com

ADVANCED
MATERIALS
TECHNOLOGIES

www.advmattechnol.de

Figure 7. 3D-TESMs from different lines show variable acute responses to caffeine and clenbuterol. A) Representative twitch force curves for line 1, before and after administration of 100 µM caffeine at D14. Noticeable is the presence of spontaneous twitches occurring between EPS-induced ones. B) Representative force curves for line 2. No spontaneous contractions are detected. C) Representative force curves for line 3. As for line 1, spontaneous twitches are detected. Gaps in the *x* axes of all the previous graphs indicate the time needed to administer the drug. D) Relative twitch force change from baseline for each line after administration of 100 µM caffeine. E–G) Relative tetanic force change from baseline in the three lines after acute administration of 50 µM clenbuterol. All the lines display a marked transient reduction in maximal force, with lines 1 and 2 showing the largest decrease. All lines show complete recovery of force after the drug washout. $n = 4$–8. Line 3 shows a significant increase in force compared to baseline after washout (P < 0.05). Error bars are shown as mean ±SD. H–J) Representative overlapping tetani curves for the three lines, before and after treatment with 50 µM clenbuterol. The tetanus curve after acute clenbuterol shows a characteristic "inverted" morphology in all the lines.
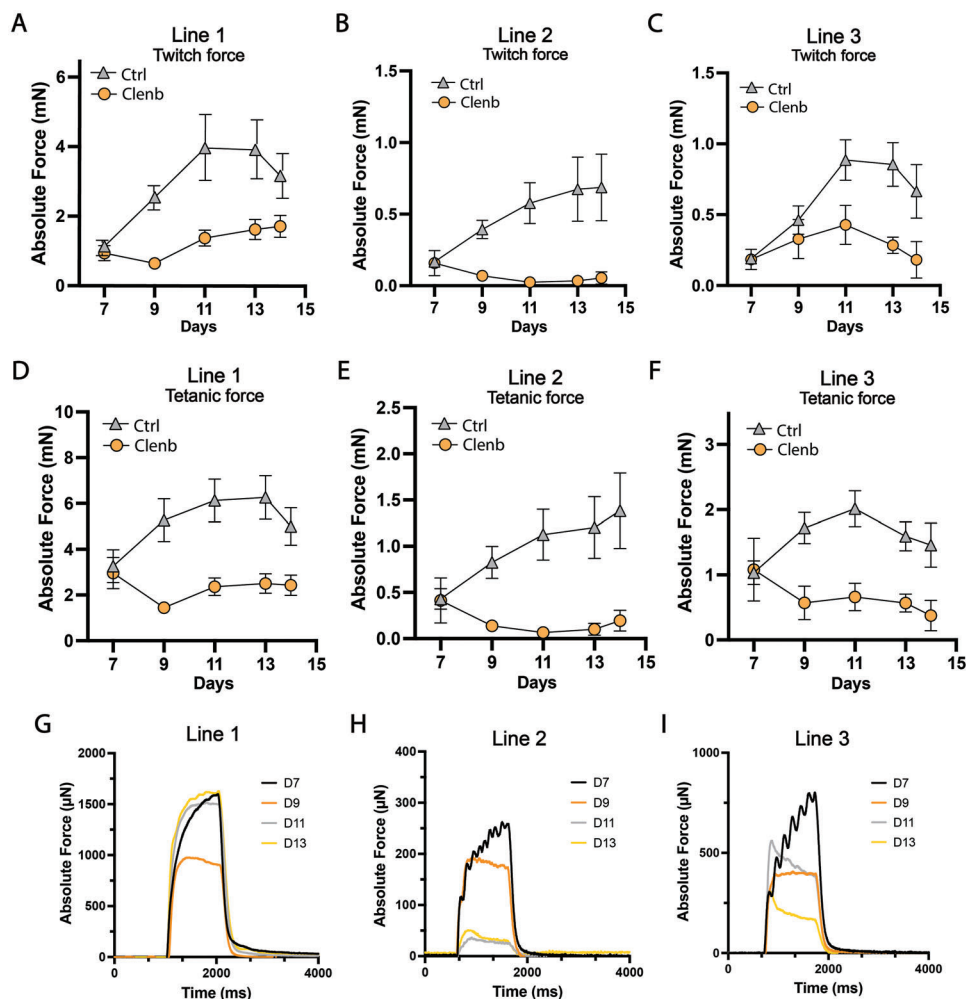
**ADVANCED
SCIENCE NEWS**

www.advancedsciencenews.com

**ADVANCED
MATERIALS
TECHNOLOGIES**

www.advmattechnol.de

Figure 8. 3D-TESMs from different lines show a distinct force reduction pattern during chronic clenbuterol treatment. A-B) Absolute twitch force of the three lines with (Clenb) or without (Ctrl) chronic administration of 10 μM clenbuterol for one week. In all lines, the drug induces marked and sustained force reduction, with complete recovery of initial force happening only in line 1 in the latest time points. D–F) Same as (A-C), but for tetanic force. $n = 4$. The behavior of the lines follows that of twitch contractions, with line 1 almost completely able to recover the initial tetanic force. Error bars are shown as mean ±SD. G) Representative tetani curves for line 1, overlapping from D7 to D13. The characteristic clenbuterol-induced shape is visible from D9 and gradually disappears towards D13. H,I) Same as (G) but for lines 2 and 3. In this case, the lines continue to show the clenbuterol-induced shape until D13.

shape until the last day of recording (Figure 8H,I). Regardless of the effects on absolute force and tetanus shape, chronic treatment with clenbuterol appeared to negatively impact the quality of the 3D-TESMs, inducing damage to the myotubes architecture when compared with controls, although with variability among the lines (Figure S5, Supporting Information).

3. Discussion

The technology presented in this work is the culmination of a process started with the development of PDMS chips equipped with flexible pillars[6] that we used to generate 3D-TESMs.[9] Such an approach aligned with the efforts of several researchers to make of in vitro engineered contractile tissues a useful and widespread tool to study muscle biology and disease. However, measuring the contractile force produced by the tissues in an accurate and continuous way is indispensable for this purpose.

In the past years progress has been made to increase the throughput of these systems, as well as the easiness of the methods to measure contractility.[2] Video imaging-based methods[2,3,5,42] rapidly spread along the classic force transducers[10–14] as ideal tools to measure contractility with the pillar-based platforms. By using mathematical formulas of the standard beam theory applied to videos of the moving pillars it is possible to estimate non-destructively the contractile force.[2] The use of pillar-based systems allowed a throughput increase compared to previous methods, reaching 96 well formats.[43] However, video imaging techniques lagged behind: some improvements on the software side were made to increase the output capacity,[3] but limitations such as low resolution and cumbersome equipment still remain. The need for better systems offered the opportunity to investigate alternative approaches. However, often the result was sacrificing user-friendliness in order to achieve automation and multiplexing.[44–46]

**ADVANCED
SCIENCE NEWS**

www.advancedsciencenews.com

**ADVANCED
MATERIALS
TECHNOLOGIES**

www.advmattechnol.de

In this study, we show the characterization of the Cuore: a 24-well-format system that can be used for the accurate and real-time measurement of contractility of 3D-engineered tissues in vitro. The system uses the principle of light interferometry with optical fiber sensors to detect the movement of cantilevers to which a contractile tissue is anchored. Because of this principle, any engineered tissue capable of spontaneous or induced contractility (e.g., cardiac muscle, skeletal or smooth muscle) can be analyzed. To our knowledge, this is the first time that this technology has been used in the field of muscle tissue engineering.

Here, we used our previously optimized highly contractile engineered skeletal muscles generated from hiPSC-derived myogenic progenitors,[7–9] to show the capability and sensitivity of the technology. Using the electrodes already integrated into the Cuore, we induced the tissues to perform twitch and tetanic contractions that we used to characterize their contractile properties. The technology allows for continuous and multiplexed recording of contractile activity of multiple tissues at the time, additionally, because of the nature of the optical sensors employed, the limit of 24 tissues could be theoretically further extended by coupling multiple Smartlids in parallel. In general, substantial amounts of data can be generated, exported, and analyzed to extrapolate peak force, contraction times, and relaxation times. With this approach it was possible to analyze the specific response of three lines, derived from three independent donors, to different EPS protocols; contraction force and time were measured continuously over the course of a week; finally, we used drugs that act on EC-coupling to observe changes in contractility in a short and long time-frame. Most of the approaches currently employed in the field would require an end-point, out of the incubator experiment to measure force. This requires the operator to also increase the number of samples needed to measure the same effect at different time points. In the case of the Cuore, being able to stimulate and record the same tissue multiple times inside the incubator, allows not only to follow the tissue development over time but also to reduce the need for additional samples. By testing increasing ramps of voltage, pulse amplitude, and frequency, an optimal combination of EPS parameters was used to produce trains of fully fused tetani, with maximal force output and without irreversibly damaging the tissues. At the same time, characteristic patterns of spontaneous contractility were recorded: in different cell lines they emerged at different time points, but they generally increased intensity and engaged more regular frequencies over time. This particular phenomenon can be considered a signature of the maturation of the 3D-TESMs over time,[19,37,47–51] as well as a specific developmental fingerprint of cell lines derived from different donors. A crucial aspect of personalized medicine is in fact the patient-to-patient variation in drug response, reflective of the variability of human individuals and populations.[52,53] Revealing this treatment response variability is essential for the success of an in vitro model in pertinent drug studies. A system that can reliably provide these insights would be a boost to the application of organs-on-chips in preclinical studies.

Thanks to the high scanning frequency that can be achieved with light interferometry sensors, the signal can generate traces comprising thousands of points per second. In this way, it is possible to record even considerably subtle details of the contraction curve, otherwise lost or demanding to obtain with other methods.[2,3,42,45,50,52] The spontaneous contractility displayed by the 3D-TESMs in the first days of culture often reached extremely low peaks that could still be detected over the noise baseline. Furthermore, because the system allows live observation of the tissues with standard or fluorescence microscopy, EPS and force recording can be coupled to other readouts such as live Ca^{2+} flux imaging. This can be particularly useful, as specific intracellular calcium kinetics and dynamics have a strict correlation with contractility and force production. As an example, the fine changes detected in the "sagged" curve generated after acute administration of clenbuterol show a level of detail previously observed only with traces from fluorescence Ca^{2+} recordings.[19,55] To our knowledge, this sensitivity is unmatched even by more recent approaches.[56] The Cuore was developed having clearly in mind the unsettled needs emerging in the field of cardiac and skeletal muscle research. From basic biology studies to drug testing and screening, the hardware here presented allows precise and reproducible analysis of the functionality of in vitro 3D contractile tissues. Furthermore, the integration of electrical stimulation and continuous recording presents new opportunities for utilizing the technology, such as investigating the impact of exercise training protocols on the functionality and maturation of 3D-TESMs. The precision, the integration of sensors and electrodes, and the non-invasiveness that allows to record contractility over different time scales, make this technology especially ideal for testing drug responses. The ability to monitor real-time changes in contractility in response to drugs makes the system an appealing option for preclinical drug studies utilizing in vitro tissue-engineered models of skeletal and cardiac muscle.

4. Experimental Section

Generation of Myogenic Progenitors lines: Myogenic Progenitors (MPs) lines were generated according to an optimization[9] of a previously published protocol.[7,8] Briefly, the three healthy hiPSCs lines underwent a transgene-free, small molecules-based myogenic differentiation protocol of the duration of 38–39 days. hiPSCs were initially seeded on plates coated with LN521 (BioLamina); the basic medium used for the myogenic differentiation was DMEM/F12 (Gibco, Waltham, MA), supplemented with 1% Penicillin-Streptomycin (P/S, Gibco), 1% KnockOut Serum Replacement (KOSR, Gibco) and 1% Insulin-Transferrin-Selenium (ITS-X, Gibco). CHIR99021 (8 µM, Axon Medchem) was added for the first 2 days of culturing, subsequently, bFGF2 (20 ng mL^{-1}, Preprotech, Rocky Hill, NJ) was added until day 17. During the last weeks, only a basic medium was used. The medium was refreshed daily for the entire duration of the protocol. At the end of the differentiation protocol, MPs were sorted using a previously published FACS protocol (ref). Freshly sorted MPs were then plated on plates coated with ECM extract (1:200 diluted, Sigma-Aldrich, E6909) cultured in MPs proliferation/growth medium (GM), consisting of DMEM (Gibco) supplemented with 4.5 g L^{-1} of glucose, glutamine, 10% FBS, 1% P/S and 100 ng mL^{-1} bFGF2. Cells were passaged after reaching 70% confluence. For passaging and harvesting, cells were detached with TrypLE reagent (Gibco) diluted 1:1 with PBS (Gibco) at 37 °C and 5% CO_2.

Generation of 3D-TESMs using the Cuore Smartlid: 3D-TESMs were generated according to our previously published protocol.[6,9] In summary, MPs (12×10^6 mL^{-1}) were mixed with a hydrogel formulation consisting of 10% v/v fibrinogen (dissolved in DMEM, final concentration 2 mg mL^{-1}, Sigma-Aldrich), 20% v/v Matrigel^O Growth Factors-Reduced (Corning), 69% v/v GM and 1% v/v Thrombin (dissolved in 0.1% BSA, final concentration 0.5 U mL^{-1}, Sigma-Aldrich) for a total volume of 50 µL. MPs were resuspended in GM, mixed with the hydrogel, and the resulting cell-hydrogel mix was pipetted directly inside the 3D-TESMs generation chambers, pre-treated with Pluronic F-127 (Sigma-Aldrich) for 1 h at

RT (Day −2, D-2). The chambers were previously fabricated using PDMS (origin) and a custom-built mold: uncured PDMS was poured inside each well of a 24 w plate, subsequently, the mold was placed on top of the 24 w plate, with 24 structures protruding inside each well, each structure having the shape of a culture chamber. After curing of PDMS (3 h at 70 °C), the mold was removed and the 24 w plate with chambers was sterilized by being washed with 70% ethanol (EtOH) for 15′, washed 3x with PBS, and finally placed under UV-light for 15′. Immediately after pipetting the cell-hydrogel mix, the Cuore Smartlid (Optics 11 – Life, Amsterdam, NL) was assembled by placing the 24w plate inside the bottom base and connecting it with the upper optical fibers plate equipped with a complete set of 24 couples of stainless-steel cantilevers. A single set of 2 cantilevers, one stiff/unmovable and one thin and flexible, coupled with an optical fiber sensor tip, make a Tissue Sensing Unit (TSU). In a TSU, the tissue will form by wrapping around the tips of the cantilevers, which act as tendon-like attachment points. The Cuore was then closed and placed on top of a shaker at 60 rpm (Celltron orbital shaker, Infors HT, Switzerland) inside a cell culture incubator set at 37°C and 5% CO$_2$ for 20′ in order to let the hydrogel solidify enough before providing the newly formed tissues with GM supplemented with 1.5 mg mL^{-1} 6-aminocaproic acid (6-ACA, Sigma-Aldrich). After 48 h (D0), GM was replaced with 3D-TESMs differentiation medium #1 (DM#1), consisting of DMEM supplemented with 4.5 g mL^{-1} glucose, 1% P/S, 1% KOSR, 1% ITS-X and 2 mg mL^{-1} 6-ACA. At this point, the 24w plate with PDMS culture chambers can be swapped for a new, standard 24w plate. After 3 days (D3), half the volume of DM#1 was replaced by DM#2, which formulation differs from DM#1 by the concentration of KOSR increasing from 1% to 20%, which is supposed to improve contractility as suggested by previous studies.[55,56] After this point, half medium was refreshed every other day for the rest of the experiment.

Drugs Experiments: Caffeine (C0750-100G, Sigma-Aldrich) was dissolved in sterile H$_2$O at a stock concentration of 50 mM and provided to the 3D-TESMs at concentrations of 100 µM (D7 or D14) and 1 mM (D7), diluted in warm DM#2. In the case of sequential administration of an additional drug, a washout step was performed: medium containing caffeine was removed, and tissues were washed once with warm PBS before a volume of new warm DM medium was provided. An eventual new drug was administered within a few minutes after the washout step. Verapamil (V4629-1G, Sigma-Aldrich) was dissolved in DMSO at a stock concentration of 10 mM and provided to the tissues at concentrations of 1 µM (D7) and 10 µM (D7 or D14), diluted in warm DM#2. Clenbuterol (origin) was dissolved in DMSO at a stock concentration of 10 mM and provided to 3D-TESMs at a concentration of 50 µM for acute effects experiments (D7) and 10 µM for chronic effects experiments (D7-14). In both cases, the medium used for experiments involving Clenbuterol was DM#1. For chronic effects experiments, the medium was half-refreshed every other day, with a new dose of the drug accounting for the total volume. In all drug experiments, 3D-TESMs were kept at 37 °C and 5% CO$_2$ during stimulation and force measurement.

Electrical Stimulation: In order to perform electrical stimulation from D7, the electrode board (Optics 11 – Life) was included as an additional component of the Cuore Smartlid. The board consisted of 24 couples of carbon plate electrodes distancing 2 cm from each other (anode-cathode), disposed at an orientation parallel to the major longitudinal axes of the tissue. The electrode board was connected to an external pulse generator (Optics 11 – Life) through a 32-pin connector. The pulse generator operated at a maximum of 100 mA at ±12 V and can generate pulses over 200 Hz. Electric fields with square wave pulses ranging from 2 V to 5 V in amplitude, pulse widths of 5–10 ms, and frequencies ranging from 20–75 Hz were utilized to assess the contraction response of tissues to electrical stimuli. For standard force measurements, a stimulation protocol of 5 V, 10 ms pulse amplitude, and either 1 Hz or 50 Hz was employed.

To elicit twitch contractions, trains of 1 Hz pulses were applied for 20 s, resulting in 20 twitches. To induce tetanic contractions, trains of 3 × 50 Hz tetani were applied for a total of 1 s per stimulus, with a 30 s interval between each stimulus. Tissues were subjected to EPS for only a few minutes at every time point. The stimulation board with electrodes was washed in distilled sterile water and EtOH in between every stimulation time point.

Force and Contraction Dynamics Measurement Using the Cuore Smartlid: The Cuore Smartlids utilized an optical fiber-based technology and employed a Fabry-Perot interferometer to measure the absolute contractile force generated by electrical stimulation of 3D-TESMs. Briefly, an IR broadband laser source was directed through fiber optics toward the flexible cantilever of each Tissue Slice Unit (TSU), with the IR light reflecting at the end of the optical fiber and orthogonally on the moving cantilever. The cavity size, which was defined by the distance between these reflective surfaces, determines the interference pattern, which was recorded with a spectrometer. Optics11Life's DeltaSens interferometer system was used to track the interference pattern over time, enabling the measurement of the movement of multiple tissues in parallel.

The Estimated Contractile Force (ECF) was determined by the deflection and material properties of the cantilever, where the tissue was attached to the bottom of the cantilever, and the measurement point was in between the anchor point and the attachment point of the muscle bundle. The resulting ECF was determined by the equation reported below. Where (*E*) is the elastic modulus, (*w*) is the width, (*t*) is the thickness, (*x*) is the measuring height of displacement on the cantilever, and (*l*) is the length to the attachment point of tissue with respect to the anchor point of the cantilever (Figure S2D, Supporting Information).

$$K_{measured} = \frac{E \cdot w \cdot t^3}{2x^2 \cdot (3l - x)}, \ with \ x < l \tag{1}$$

Live visualization of the baseline ECF and electrical signal amplitude was displayed in the control software of the Cuore (Optics 11 – Life) and stored. This allowed for the analysis of time-dependent contraction dynamics such as Time-to-Peak Force (TtP) (tpeak – t0), Relaxation Time (t1 – tpeak), total contraction time (TtP + Relaxation Time), (maximum) contraction velocity, and (maximum) relaxation velocity. The absolute contractile force was calculated as the average of the peak forces of the total contractile events in all analyses. The cantilevers used in the study were calibrated by stiffness testing, by deforming them repeatedly with a micromanipulator and measuring the resulting force output. The resulting variance was just under 5%. Furthermore, for earlier cantilever designs produced to prototype and optimize our final model, the calibration based on a gravitational method was also evaluated for calibration that showed a variance of <10% on the overall deflection test.

Live Imaging and Measurement of Ca^{2+} Signal: A solution based on DMEM High Glucose without phenol red, containing the fluorescently labeled calcium indicator Fluo-4 AM (Thermo Fisher Scientific) and 0.02% Pluronic F-127 was used for the Ca^{2+} imaging experiments. Tissues were incubated with the solution for 1 h at 37 °C and 5% CO$_2$ and were then washed three times with warm DMEM without phenol red before imaging. An Echo Revolve (Bico) fluorescence microscope was used to live-image the 3D-TESMs while they were electrically stimulated and recorded using the DeltaSens system. Light intensity and exposure were maintained constant and on under-bleaching levels throughout the experiment. Videos were then analyzed using a custom script Python program that automatically detected changes in pixel intensity over the different frames comprising the videos. The same script was also used to time-wise overlap the fluorescence signal and the force traces obtained using the Cuore.

Immunohistochemistry: Samples were fixed in 4% paraformaldehyde (PFA, Sigma-Aldrich) for 1 h at RT and then washed with PBS for three times. For whole-mount immunostaining, fixed samples were first subjected to a permeabilization/blocking step in a solution containing 0.5% Triton-X in PBS, 3% BSA in PBS, 0.1% Tween 20 in PBS on agitation (all Sigma-Aldrich), for 1 h at RT. After washing with PBS, samples were incubated with primary antibody for titin, 9D 10-s (1:50, DSHB, IA), in 0.1% Triton-X in PBS, 0.1% BSA in PBS, 0.1% Tween 20 in PBS at 4 °C, for 1 h. Before incubation with the secondary antibody Alexa Fluor 488 (1:500, Thermo Fisher Scientific, Waltham, MA), samples were washed in 0.1% Tween in PBS for 2 min and subsequently in PBS for 2 min. Secondary antibodies were diluted in the same solution used for the primary antibodies and samples were incubated for 1 h at RT. Lastly, nuclear staining was performed through incubation with DAPI (1:10 000, Sigma-Aldrich)

at RT for 15 min followed by washing in PBS. Samples were kept in PBS at 4 °C before imaging.

Imaging Analysis of IF-Stained Samples: Stained samples were imaged using a Leica TCS SP5 confocal microscope (Leica, Germany) equipped with LAS software (Leica, Germany), using 10× and 20× magnifications. Images were then analyzed using ImageJ version 1.52i.

Statistical Analysis: Statistical analysis was performed using GraphPad Prism (v.8.0) software. One- or two-way ANOVA was used to assess statistical significance after verifying the normal distribution of data and multiple correction testing was performed with the Tukey method.

Supporting Information

Supporting Information is available from the Wiley Online Library or from the author.

Acknowledgements

Conflict of Interest

Matthias Haalstra, Ramkumar Raghuraman, and Kevin Bielawski are employees of Optics11 Life B.V.

Data Availability Statement

The data that support the findings of this study are available from the corresponding author upon reasonable request.

Keywords

[1] A. Khodabukus, N. Prabhu, J. Wang, N. Bursac, *Adv. Healthcare Mater.* **2018**, *7*, 1701498.

[2] H. Vandenburgh, J. Shansky, F. Benesch-Lee, V. Barbata, J. Reid, L. Thorrez, R. Valentini, G. Crawford, *Muscle Nerve* **2008**, *37*, 438.

[3] L. Sala, B. J. Van Meer, L. G. J. Tertoolen, J. Bakkers, M. Bellin, R. P. Davis, C. Denning, M. A. E. Dieben, T. Eschenhagen, E. Giacomelli, C. Grandela, A. Hansen, E. R. Holman, M. R. M. Jongbloed, S. M. Kamel, C. D. Koopman, Q. Lachaud, I. Mannhardt, M. P. H. Mol, D. Mosqueira, V. V. Orlova, R. Passier, M. C. Ribeiro, U. Saleem, G. L. Smith, F. L. Burton, C. L. Mummery, *Circ. Res.* **2018**, *122*, e5.

[4] M. Ebrahimi, H. Lad, A. Fusto, Y. Tiper, A. Datye, C. T. Nguyen, E. Jacques, L. A. Moyle, T. Nguyen, B. Musgrave, C. Chávez-Madero, A. Bigot, C. Chen, S. Turner, B. A. Stewart, E. Pegoraro, L. Vitiello, P. M. Gilbert, *Acta Biomater.* **2021**, *2*, 27.

[5] A. Hansen, A. Eder, M. Bönstrup, M. Flato, M. Mewe, S. Schaaf, B. Aksehirlioglu, A. Schwörer, J. Uebeler, T. Eschenhagen, *Circ. Res.* **2010**, *107*, 35.

[6] A. Iuliano, E. Van Der Wal, C. W. B. Ruijmbeek, S. L. M. In 'T Groen, W. W. M. P. Pijnappel, J. C. De Greef, V. Saggiomo, *Adv. Mater. Technol.* **2020**, *5*, 2000344.

[7] E. Van Der Wal, P. Herrero-Hernandez, R. Wan, M. Broeders, S. L. M. In 'T Groen, T. J. M. Van Gestel, W. F. J. Van Ijcken, T. H. Cheung, A. T. Van Der Ploeg, G. J. Schaaf, W. W. M. P. Pijnappel, *Stem Cell Rep.* **2018**, *10*, 1975.

[8] E. van der Wal, A. J. Bergsma, T. J. M. Van Gestel, S. L. M. In 'T Groen, H. Zaehres, M. J. Araúzo-Bravo, H. R. Schöler, A. T. Van Der Ploeg, W. W. M. P. Pijnappel, *Mol. Ther. – Nucleic Acids* **2017**, *7*, 101.

[9] E. van der Wal, A. Iuliano, S. M. L. in 't Groen, A. P. Bholasing, D. Priesmann, P. Sharma, B. den Hamer, V. Saggiomo, M. Kruger, W. M. P. Pijnappel, W. J. de Greef, *Stem Cell Reports unpublished* **2023**.

[10] A. Khodabukus, L. Madden, N. K. Prabhu, T. R. Koves, C. P. Jackman, D. M. Muoio, N. Bursac, *Biomaterials* **2018**, *198*, 259.

[11] M. Juhas, N. Abutaleb, J. T. Wang, J. Ye, Z. Shaikh, C. Sriworarat, Y. Qian, N. Bursac, *Nat. Biomed. Eng.* **2018**, *2*, 942.

[12] B. Liau, N. Christoforou, K. W. Leong, N. Bursac, *Biomaterials* **2011**, *32*, 9180.

[13] J. Wang, C. J. Zhou, A. Khodabukus, S. Tran, S.-O.h Han, A. L. Carlson, L. Madden, P. S. Kishnani, D. D. Koeberl, N. Bursac, *Commun Biol* **2021**, *4*, 524.

[14] Z. Chen, B. Li, R.-Z. Zhan, L. Rao, N. Bursac, *Sci. Adv.* **2021**, *7*, eabd9502.

[15] W. Bauer, M. Weber, S. Chanbai, *Encycl. Tribol.* **2013**, 4115.

[16] M. Berardi, K. Bielawski, N. Rijnveld, G. Gruca, H. Aardema, L. Van Tol, G. Wuite, B. I. Akca, *Commun. Biol.* **2021**, *4*, 610.

[17] A. Hansen, A. Eder, M. Bönstrup, M. Flato, M. Mewe, S. Schaaf, B. Aksehirlioglu, A. Schwörer, J. Uebeler, T. Eschenhagen, *Circ. Res.* **2010**, *107*, 35.

[18] E. Van Der Wal, P. Herrero-Hernandez, R. Wan, M. Broeders, S. L. M. In 'T Groen, T. J. M. Van Gestel, W. F. J. Van Ijcken, T. H. Cheung, A. T. Van Der Ploeg, G. J. Schaaf, W. W. M. P. Pijnappel, *Stem Cell Rep.* **2018**, *10*, 1975.

[19] B. E. Flucher, S. B. Andrews, *Cell Motil. Cytoskeleton* **1993**, *25*, 143.

[20] D. Neyroud, A. J. Cheng, C. Donnelly, N. Bourdillon, A.-L. Gassner, L. Geiser, S. Rudaz, B. Kayser, H. Westerblad, N. Place, *Am. J. Physiol. Physiol.* **2019**, *316*, C246.

[21] D. G. Allen, H. Westerblad, *J. Physiol.* **1995**, *487*, 331.

[22] M. A. Hughes, R. M. Downs, G. W. Webb, C. L. Crocker, S. T. Kinsey, B. L. Baumgarner, *J. Muscle Res. Cell Motil.* **2017**, *38*, 201.

[23] D. S. Enyart, C. L. Crocker, J. R. Stansell, M. Cutrone, M. M. Dintino, S. T. Kinsey, S. L. Brown, B. L. Baumgarner, *Physiol. Rep.*, *8*, 14340.

[24] M. Tarnopolsky, C. Cupido, *J. Appl. Physiol.* **2000**, *89*, 1719.

[25] J. K. Schnuck, L. M. Gould, H. A. Parry, M. A. Johnson, N. P. Gannon, K. L. Sunderland, R. A. Vaughan, *J. Physiol. Biochem.* **2018**, *74*, 35.

[26] T. E. Graham, L. L. Spriet, *J. Appl. Physiol.* **1995**, *78*, 867.

[27] D. Neyroud, A. J. Cheng, C. Donnelly, N. Bourdillon, A.-L. Gassner, L. Geiser, S. Rudaz, B. Kayser, H. Westerblad, N. Place, *Am. J. Physiol. Cell Physiol.* **2019**, *316*, C246.

[28] H. H. Valdivia, C. Valdivia, J. Ma, R. Coronado, *Biophys. J.* **1990**, *58*, 471.

[29] J.-P. Galizzi, M. Fosset, M. Lazdunski, *Eur. J. Biochem.* **1984**, *144*, 211.

[30] I.i. L. Sasse, R. Hajer, *J. Vet. Pharmacol. Ther.* **1978**, *1*, 241.

[31] B. M. Pluim, O. De Hon, J. B. Staal, J. Limpens, H. Kuipers, S. E. Overbeek, A. H. Zwinderman, R. J. P. M. Scholten, *Sport. Med.* **2011**, *41*, 39.

**ADVANCED
SCIENCE NEWS**

www.advancedsciencenews.com

**ADVANCED
MATERIALS
TECHNOLOGIES**

www.advmattechnol.de

[32] P. A. Maclennan, R. H. Edwards, *Biochem. J.* **1989**, *264*, 573.

[33] J. Meister, D. B. J. Bone, J. R. Knudsen, L. F. Barella, T. J. Velenosi, D. Akhmedov, R. J. Lee, A. H. Cohen, O. Gavrilova, Y. Cui, G. Karsenty, M. Chen, L. S. Weinstein, M. Kleinert, R. Berdeaux, T. E. Jensen, E. A. Richter, J. Wess, *Nat. Commun.* **2022**, *13*, 1.

[34] S. Jessen, S. A. Solheim, G. A. Jacobson, K. Eibye, J. Bangsbo, N. B. Nordsborg, M. Hostrup, *Drug Test. Anal.* **2020**, *12*, 610.

[35] S. I. Head, T. N.v Ha, *Clin. Exp. Pharmacol. Physiol.* **2011**, *38*, 638.

[36] E. E. Dupont-Versteegden, M. S. Katz, R. J. Mccarter, *Muscle Nerve* **1995**, *18*, 1447.

[37] T. Morita, K. Kihara, H. Nagamatsu, H. Oshima, T. Kishimoto, *J. Smooth Muscle Res.* **1995**, *31*, 119.

[38] A. J. Bakker, S. I. Head, A. C. Wareham, D. G. Stephenson, *Am. J. Physiol. – Cell Physiol.* **1998**, *274*, 43.

[39] P. Sirvent, A. Douillard, O. Galbes, C. Ramonatxo, G. Py, R. Candau, A. Lacampagne, *PLoS One* **2014**, *9*, e100281.

[40] N. D. Duncan, D. A. Williams, G. S. Lynch, *Clin. Sci.* **2000**, *98*, 339.

[41] C. F. Kearns, K. H. McKeever, K. Malinowski, M. B. Struck, A. B. E. Takashi, *J. Appl. Physiol.* **2001**, *91*, 2064.

[42] M. Ebrahimi, H. Lad, A. Fusto, Y. Tiper, A. Datye, C. T. Nguyen, E. Jacques, L. A. Moyle, T. Nguyen, B. Musgrave, C. Chávez-Madero, A. Bigot, C. Chen, S. Turner, B. A. Stewart, E. Pegoraro, L. Vitiello, P. M. Gilbert, *Acta Biomater.* **2021**, *132*, 227.

[43] M. E. Afshar, H. Y. Abraha, M. A. Bakooshli, S. Davoudi, N. Thavandiran, K. Tung, H. Ahn, J. Ginsberg, P. W. H. Zandstra, P. M. Gilbert, *Sci. Reports* **2020**, *10*, 1.

[44] H. Kim, M.-C. Kim, H. H. Asada, *Sci. Rep.* **2019**, *9*, 2732.

[45] S. A. Najjar, A. S. T. Smith, C. J. Long, C. W. Mcaleer, Y. Cai, B. Srinivasan, C. Martin, H. H. Vandenburgh, J. J. Hickman, *Biotechnol. Bioeng.* **2020**, *117*, 736.

[46] M. A. Ortega, X. Fernández-Garibay, A. G. Castaño, F. De Chiara, A. Hernández-Albors, J. Balaguer-Trias, J. Ramón-Azcón, *Lab Chip* **2019**, *19*, 2568.

[47] P. G. De Deyne, *Am. J. Physiol. – Cell Physiol.* **2000**, *279*, C1801.

[48] R. G. Dennis, P. E. Kosnik II, *Vitr. Cell. Dev. Biol. – Anim.* **2000**, *36*, 327.

[49] W. Bian, N. Bursac, *Biomaterials* **2009**, *30*, 1401.

[50] L. Madden, M. Juhas, W. E. Kraus, G. A. Truskey, N. Bursac, *elife* **2015**, *4*, 04885.

[51] M. Weitkunat, M. Lindauer, A. Bausch, F. Schnorrer, *Dev* **2017**, *144*, 1261.

[52] A. G. Madian, H. E. Wheeler, R. B. Jones, M. E. Dolan, *Trends Genet.* **2012**, *28*, 487.

[53] D. M. Roden, A. L. George Jr, *Nat. Rev. Drug Discovery* **2002**, *11*, 37.

[54] A. Hansen, A. Eder, M. Bönstrup, M. Flato, M. Mewe, S. Schaaf, B. Aksehirlioglu, A. Schwörer, J. Uebeler, T. Eschenhagen, *Circ. Res.* **2010**, *107*, 35.

[55] S. I. Head, T. N. Ha, *Clin. Exp. Pharmacol. Physiol.* **2011**, *38*, 638.

[56] A. S. T. Smith, S. M. Luttrell, J. B. Dupont, K. Gray, D. Lih, J. W. Fleming, N. J. Cunningham, S. Jepson, J. Hesson, J. Mathieu, L. Maves, B. J. Berry, E. C. Fisher, N. J. Sniadecki, N. A. Geisse, D. L. Mack, *J. Tissue Eng.* **2022**, *13*.

[57] B. Xu, A. Magli, Y. Anugrah, S. J. Koester, R. C. R. Perlingeiro, W. Shen, *Biomaterials* **2018**, *183*, 54.

[58] B. Xu, M. Zhang, R. C. R. Perlingeiro, W. Shen, *Adv. Biosyst.* **2019**, *3*, 1900005.

2300845 (15 of 15)